JOURNAL OF THERMOPHYSICS AND HEAT TRANSFER
Vol. 20, No. 3, July–September 2006

Flows Induced by Thermoacoustic Waves in an Enclosure: Effects of Gravity

Yiqiang Lin* and Bakhtier Farouk†
Drexel University, Philadelphia, Pennsylvania 19104
and
Elaine S. Oran‡
U.S. Naval Research Laboratory, Washington, D.C. 20375

The effect of gravity on the generation and propagation of flows induced by thermoacoustic waves in an enclosure was numerically investigated. The compressible unsteady Navier–Stokes equations were solved by combining a flux-corrected transport algorithm for the convection terms and by a central differencing scheme for the viscous and conduction terms. In the simulations, the left wall of the enclosure is heated rapidly either in a spatially uniform or a nonuniform manner, whereas the right wall is held at the initial temperature of the gas. The upper and lower walls of the enclosure are insulated. At zero gravity, the spatially nonuniform heating generates a vortical flow in the enclosure, similar to that found in buoyancy-induced flows in a side-heated enclosure. For the conditions considered, the strength of the flows induced by the thermoacoustic waves is comparable to the flows induced by buoyancy.

Nomenclature

A = overheat ratio
a = acoustic speed, m/s
E = total energy, J/kg
e = internal energy, J/kg
g = gravitational acceleration, m/s^2
k = thermal conductivity, W/m · K
L = dimension of the enclosure, m
p = pressure, Pa
R = specific gas constant, J/kg · K
T = temperature, K (or °C)
t = time, s
u = velocity component in the horizontal direction, m/s
v = velocity component in the vertical direction, m/s
x = horizontal direction, m
y = vertical direction, m
μ = dynamic viscosity, N · s/m^2
ρ = density, m^3/kg
τ = time constant, s

Subscripts

B = bottom wall
L = left wall
n = normal to the wall
R = right wall
T = top wall
w = wall position
0 = initial

Received 6 June 2005; revision received 12 August 2005; accepted for publication 15 August 2005.

*Graduate Student, Department of Mechanical Engineering and Mechanics. 3141 Chestnut Street.
†Professor, Department of Mechanical Engineering and Mechanics, 3141 Chestnut Street. Senior Member AIAA.
‡Senior Scientist, Laboratory for Computational Physics and Fluid Dynamics, 4555 Overlook Avenue S.W. Fellow AIAA.

I. Introduction

WHEN a compressible fluid within an enclosure is subjected to a rapid temperature increase along a solid wall, the fluid in the immediate vicinity of the wall expands. This gives rise to a fast increase in the local pressure and leads to the production of pressure waves called thermoacoustic waves. These thermoacoustic waves are repeatedly reflected from the chamber walls, and a nonuniform flowfield is developed within the enclosure. This flow may cause unwanted disturbances in otherwise static processes such as cryogenic storage, or may introduce a convective heat transfer mode to the systems in zero-gravity environments where conduction and radiation are the only heat transfer modes. In near-critical fluids, which are characterized by low-heat diffusivity for conduction heat transfer, the thermoacoustic convection mode of heat transport can become very important, especially in a reduced-gravity environment.

There has been a considerable amount of analytic and some related numerical and experimental work to study one-dimensional thermoacoustic waves.[1–9] The problem of thermoacoustic waves in a quiescent semi-infinite body of a perfect gas, subjected to a step change in temperature at the solid wall, has been studied analytically[10] to determine how the sound intensity depends on the history of the wall temperature. In another work, the one-dimensional compressible flow equations were linearized and a closed-form asymptotic solution was obtained using a Laplace transform technique. A simplified model (the hyperbolic equation of conduction) for thermoacoustic motion was compared with one-dimensional Navier–Stokes equations model of the phenomena, and limitations of the simplified approach was discussed (see Ref. 1). Later a more general class of solutions for the thermoacoustic waves was obtained for step and gradual changes in the boundary temperature by using the Laplace transform method with a linear wave model (see Ref. 3). The equations of the nonlinear wave model were numerically solved using a finite difference scheme modified with a Galerkin finite element interpolation in space. A similar analysis for thermoacoustic waves in a confined medium was repeated more recently.[4] In both geometries, the analysis was limited to a gas medium with Prandtl number of 0.75. Thermoacoustic convection phenomena were experimentally investigated in a cylinder containing air with temperature measurements in normal- and reduced-gravity environment.[7] Temperature measurements were reported but no pressure measurements. Experimental measurements of pressure waves generated by rapidly heating a surface were reported by Brown and Churchill.[8]

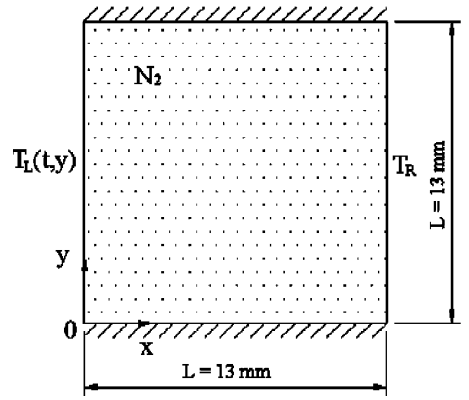

Fig. 1 Geometry and boundary conditions of problem.

Numerical studies of one- and two-dimensional thermoacoustic waves in a confined region were carried out by Ozoe et al.,[11,12] Farouk et al.,[2] and Aktas and Farouk.[13] These computational studies described finite difference solutions of the compressible Navier–Stokes equations for a gas with temperature-independent thermophysical properties. The results of Ozoe et al.,[11,12] who used an upwind scheme to solve the governing equations, shows effects of substantial numerical diffusion. Using a high-order numerical scheme, Farouk et al. predicted the early time behavior of thermoacoustic waves in a compressible fluid-filled cavity with a computational study[2] in which temperature-dependent fluid properties were used. The computational results agreed well with available experimental data in the literature. Aktas and Farouk[13] recently studied the interaction of thermoacoustic waves and buoyancy-induced flows in an enclosure with uniformly heated walls. Brown and Churchill[9] have also shown that rapid heating of a solid surface bounding a region of gas generates a slightly supersonic wave with positive amplitude in pressure, temperature, density, and mass velocity. Their one-dimensional predictions were in good qualitative agreement with prior experimental measurements of the shape, amplitude, and rate of decay of the pressure waves. In another computational study, the mechanisms of heat and mass transport in a side-heated square cavity filled with a near-critical fluid are explored,[14] with special emphasis on the interplay between buoyancy-driven convection and the piston effect.

In the present paper, flows induced by thermoacoustic waves are studied under zero and normal-gravity conditions in a square enclosure with side length $L = 13$ mm (Fig. 1). The horizontal walls of the square enclosure are adiabatic. Initially the gas and all of the walls are in thermal equilibrium; $T = T_R$ everywhere. At later times, $t > 0$, the left-wall temperature is increased to $T_L (T_L > T_R)$, either suddenly or gradually. We examine the effects of increases in temperature that are either spatially uniform or nonuniform.

II. Mathematical and Numerical Model

The generation and propagation of flows induced by thermoacoustic waves are governed by the Navier–Stokes equations for a compressible fluid. In two-dimensional Cartesian coordinates, these equations can be expressed in conservative form as

$$\frac{\partial \rho}{\partial t} + \frac{\partial (\rho u)}{\partial x} + \frac{\partial (\rho v)}{\partial y} = 0 \tag{1}$$

$$\frac{\partial (\rho u)}{\partial t} + \frac{\partial (\rho u^2)}{\partial x} + \frac{\partial (\rho uv)}{\partial y} + \frac{\partial p}{\partial x} = \frac{\partial \tau_{xx}}{\partial x} + \frac{\partial \tau_{xy}}{\partial y} \tag{2}$$

$$\frac{\partial (\rho v)}{\partial t} + \frac{\partial (\rho uv)}{\partial x} + \frac{\partial (\rho v^2)}{\partial y} + \frac{\partial p}{\partial y} = \frac{\partial \tau_{xy}}{\partial x} + \frac{\partial \tau_{yy}}{\partial y} - \rho g \tag{3}$$

$$\frac{\partial E}{\partial t} + \frac{\partial (Eu)}{\partial x} + \frac{\partial (Ev)}{\partial y} + \frac{\partial (pu)}{\partial x} + \frac{\partial (pv)}{\partial y} = \frac{\partial q_x}{\partial x} + \frac{\partial q_y}{\partial y} + \phi \tag{4}$$

where u and v are the velocity components and p is the thermal pressure.

The stress tensor τ_{ij} can be written as

$$\tau_{xx} = 2\mu \frac{\partial u}{\partial x} - \frac{2}{3}\mu \left[\frac{\partial u}{\partial x} + \frac{\partial v}{\partial y} \right] \tag{5}$$

$$\tau_{yy} = 2\mu \frac{\partial v}{\partial y} - \frac{2}{3}\mu \left[\frac{\partial u}{\partial x} + \frac{\partial v}{\partial y} \right] \tag{6}$$

$$\tau_{xy} = \tau_{yx} = \mu \left[\frac{\partial v}{\partial x} + \frac{\partial u}{\partial y} \right] \tag{7}$$

The components of the heat flux are written as

$$q_x = \lambda \frac{\partial T}{\partial x} \tag{8a}$$

$$q_y = \lambda \frac{\partial T}{\partial y} \tag{8b}$$

where λ is the thermal conductivity.

The viscous dissipation in Eq. (4) is written as

$$\phi = \frac{\partial (\tau_{xx} u + \tau_{xy} v)}{\partial x} + \frac{\partial (\tau_{yx} u + \tau_{yy} v)}{\partial y} \tag{9}$$

In addition, an equation of state for perfect gas is used to relate the temperature to the other thermodynamic characteristics,

$$p = \rho P T \tag{10}$$

The temperature dependence of the viscosity and thermal conductivity[15] are taken into account using the following polynomial expressions:

$$\mu(T) = -1.253\times10^{-6} + 8.983\times10^{-8} T - 1.139\times10^{-10} T^2 + 9.101\times10^{-14} T^3 \tag{11}$$

$$k(T) = 1.494\times10^{-4} + 1.108\times10^{-4} T - 1.045\times10^{-7} T^2 + 6.958\times10^{-11} T^3 \tag{12}$$

The governing equations (except for the diffusion terms) are discretized using a finite volume method based on the flux-corrected transport (FCT) algorithm. FCT is a high-order, nonlinear, monotone, conservative, and positivity-preserving method designed to solve a one-dimensional continuity equation or coupled continuity equations with appropriate source terms. This method has fourth-order phase accuracy and is able to resolve steep gradients with minimum numerical diffusion. In this algorithm, when a flow variable such as a density is initially positive, it remains positive during the computations and no new minimum or maximum values are introduced due to numerical errors in the calculation process. To ensure positivity and stability, a minimum amount of numerical diffusion over the stability limit is added at each time step. Further details of the FCT algorithm used here are documented in Ref. 16. The diffusion terms (the viscous term in the momentum equations and the conduction terms in the energy equation) were discretized using a second-order central-difference approach. Time-step splitting was also used to couple all of the representative physical effects.

No-slip boundary conditions were used at all solid walls. Time-dependent boundary conditions for the vertical walls and zero-gradient temperature boundary conditions at the horizontal walls were used. The treatment proposed by Poinsot and Lele[17] was followed for implementing the boundary conditions for the density. Along any solid wall, the density is calculated from

$$\left(\frac{\partial \rho}{\partial t} \right)_w + \frac{1}{a_w} \left(\frac{\partial p}{\partial n} + \rho a_w \frac{\partial u_n}{\partial n} \right)_w = 0 \tag{13}$$

where the subscript w signifies the location of the wall and n is the direction normal to the wall.

III. Results and Discussion

Numerical simulations of the flows induced by thermoacoustic waves were performed in a square enclosure filled with nitrogen gas at 1 atm and 300 K. Results were obtained for four cases: uniform impulsive heating without gravity, uniform gradual heating without gravity, spatially nonuniform gradual heating without gravity, and spatially nonuniform gradual heating with gravity.

Results of a prior investigation[2] of the very short-time behavior of the thermoacoustic waves generated by impulsive and gradual heating of a wall were in very good qualitative and quantitative agreement with the results given in the literature. In the present study, the longer-time behavior of the velocity fields, produced by either step impulsive heating or gradual heating of the left wall, was investigated under zero- and normal-gravity conditions. In a numerical method, impulsive heating can be approximated by changing the value of the temperature in the first time step. In the present computations, the first time step is small (2.81×10^{-8} s) compared to the characteristic acoustic and diffusion times in the system.

A. Uniform Impulsive Heating at Zero Gravity

For impulsive heating, the temperature of the left wall is given as

$$T_L(t) = T_0[1 + A], \qquad t \geq 0 \tag{14}$$

where the overheat ratio A is given by

$$A = (T_L - T_0)/T_0 \tag{15}$$

and is 1/3 for all cases presented for spatially uniform wall heating.

The variation of pressure at the midpoint of the enclosure is shown in Fig. 2 for early times, and a distinctive peak is observed whenever the thermoacoustic wave crosses the midpoint. This wave periodically reflects from both side walls, as seen by the multiple peaks. We have shown earlier[2] that the strength of the pressure wave is strongly correlated to the overheat ratio and pressure oscillations damp out with increasing time. Computational cells were nonuniformly distributed with fine grids in the vicinity of the boundary. The ratio of the maximum to the minimum grid size was 5.0. The results for a resolution study using three mesh sizes, 201×201, 241×241, and 281×281, are also shown in Fig. 2. The initial time step was, however, kept the same for all three mesh sizes to represent identical impulsive heating for all cases. From these tests, a mesh size of 241×241 was found to be adequate for the present computations. The time variation of the pressure and the x component of the velocity at the midpoint of the enclosure for a short time after the impulsive heating are shown in Fig. 3. The x component of the

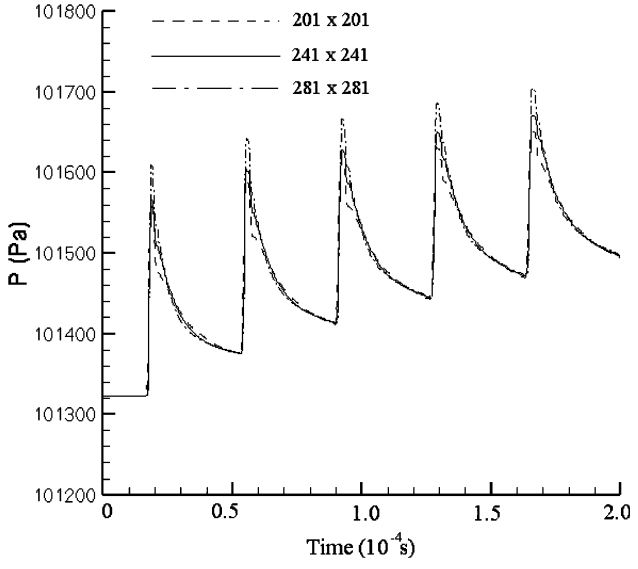

Fig. 2 Variation of pressure at midpoint of enclosure for three grid sizes, under spatially uniform impulsive heating, zero gravity.

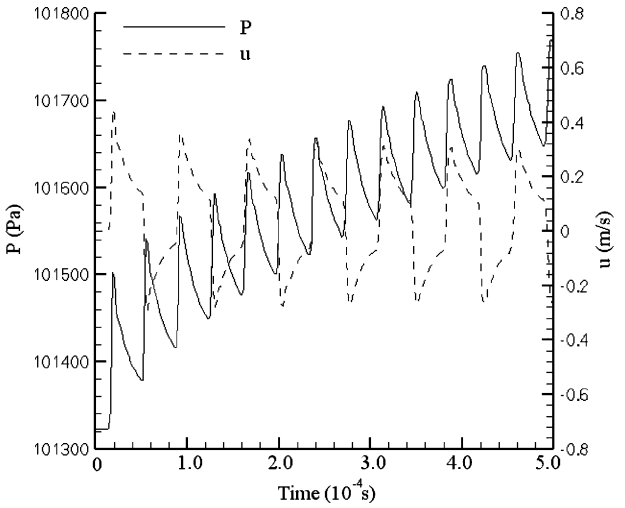

Fig. 3 Variation of pressure and x component of velocity at midpoint of enclosure for early time, under spatially uniform impulsive heating, zero gravity.

velocity fluctuates between positive and negative values, depending on the direction of the oncoming pressure wave.

The velocity vectors in Fig. 4 (at 25.78 and 100 ms) show the flowfields that developed from the wave motion created by the impulsive heating. Indeed, with spatially uniform heating and zero-gravity conditions, the flowfield is essentially symmetric along the horizontal midplane. Flow structures develop along the top and bottom left corners due to viscous interactions between the solid surfaces and bulk fluid. The strength of the flowfield decreases in time and has decreased considerably at 100 ms. In Fig. 5, we show the temporal variation of the u component of the velocity at the midpoint for 100 ms. The thermoacoustic wave undergoes many reflections from the sidewalls during this period. The dark regions reflect the highly oscillatory nature of the flowfield. The x-velocity component decays with every reflection, and by 100 ms, it becomes relatively small.

B. Spatially Uniform Gradual Heating Under Zero Gravity

The thermal inertia of walls and heating systems as well as unavoidable heat losses to the environment make it difficult in practice to generate a step change (impulsive heating) in the wall temperature. Here we study the effect of more gradual heating by using an exponential expression for the wall heating,

$$T_L(t) = T_0(1 + A\{1 - \exp[(t/\tau_h)]\}) \qquad t \geq 0 \tag{16}$$

where τ_h is a time constant. For impulsive heating, τ_h tends to zero.

Figure 6 shows the variation of the pressure and the x component of the velocity at the midpoint for early times, and with gradual wall heating. The time constant is $\tau_h = 5\tau_c$, where, τ_c is the travel time of sound waves for the length of the enclosure. Also in Fig. 6, the variation of the left wall temperature with time is shown. Comparing Fig. 6 with Fig. 3 shows that, for gradual wall heating, the thermoacoustic wave is much weaker. As shown in Fig. 6, the pressure values at the midpoint increase continuously; however, there are discrete jumps in its value each time the wave crosses the center. The effect of gradual heating on the x component of the velocity is interesting: The velocity component still fluctuates with time, but now it does not reverse sign (as shown in Fig. 3), and hence, the damping rate is slower.

Figure 7 shows velocity vectors at two different times (25.78 and 100 ms) for the case just described. The velocity field is similar to the case of impulsive heating; it is symmetric along the horizontal midplane and decays with time. Comparing Figs. 3a and 7a, we find that the flowfield induced by the impulsive heating is much stronger at 25.78 ms. The flowfields shown in Figs. 3b and 7b for 100 ms are, however, not that different. The decay rate slows down at later time, irrespective of the mode of heating. In Fig. 8, we show the temporal variation of the u-component of the velocity at the midpoint for

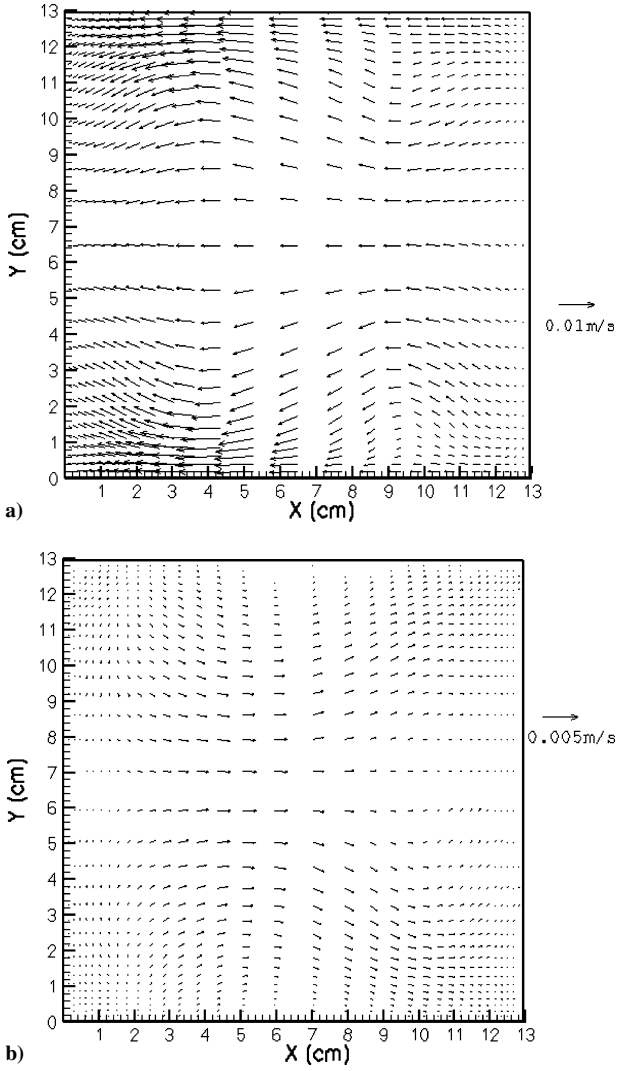

Fig. 4 Velocity vectors under spatially uniform impulsive heating, zero gravity: a) 27.58 ms and b) 100 ms.

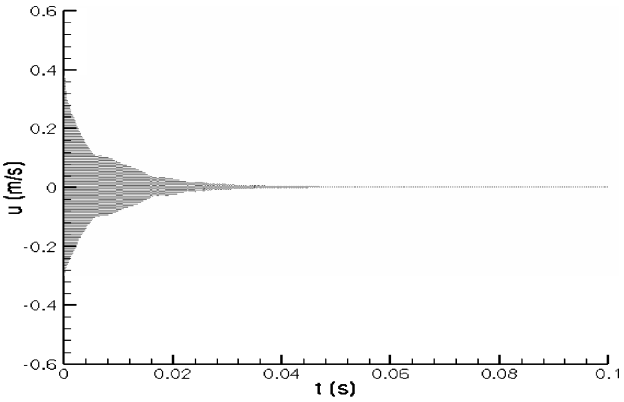

Fig. 5 Variation of x component of velocity with time at midpoint of enclosure, under spatially uniform impulsive heating, zero gravity.

100 ms for gradual heating. The dark regions in Fig. 8 again reflect the highly oscillatory nature of the flowfield. Comparing Fig. 8 with Fig. 5 shows that the x component of velocity at the midpoint at 100 ms for gradual heating is much higher than that of the impulsive heating case.

C. Spatially Nonuniform Gradual Heating at Zero Gravity

For the case of spatially nonuniform, gradual heating, the left wall temperature is now given by

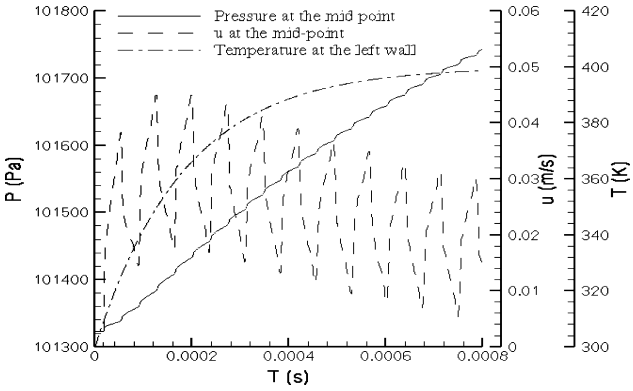

Fig. 6 Variation of pressure and x component of velocity at midpoint of enclosure for early time, under spatially uniform gradual heating $\tau_h = 5\tau_c$, zero gravity.

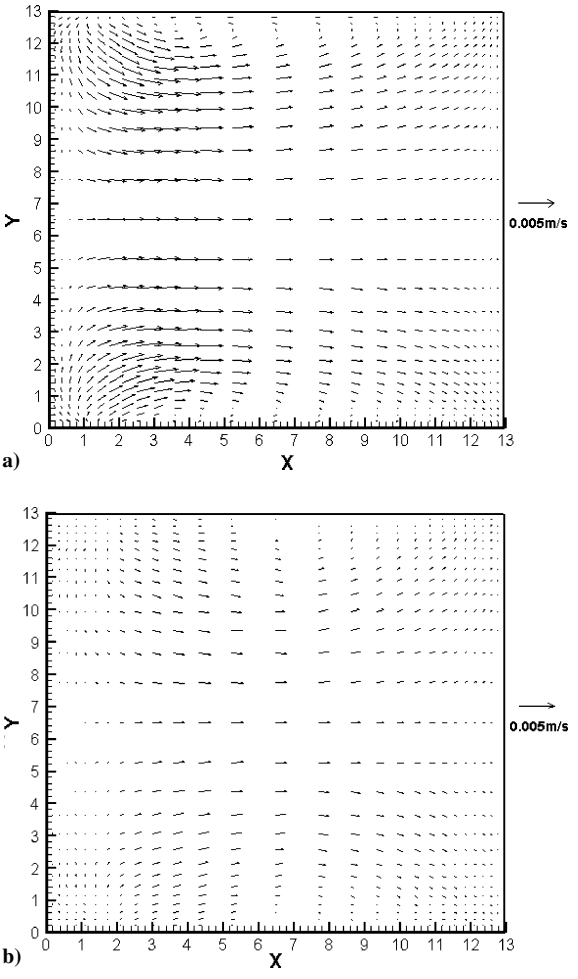

Fig. 7 Velocity vectors under spatially uniform gradual heating, $\tau_h = 5\tau_c$, zero gravity: a) = 27.58 ms and b) 100 ms.

$$T_L(t, y) = T_0(1 + 2\bar{A}\{1 - \exp[(t/\tau_h)]\}[(L - y)/L]), \qquad t \geq 0 \tag{17}$$

and so the spatial temperature distribution along the wall now varies linearly.

Figure 9 indicates the time variation of pressure along the vertical midplane ($x = L/2$) of the enclosure at three locations, $y = L/4$, $L/2$, and $3L/4$. These curves are similar to those shown earlier for spatially uniform gradual heating (Fig. 6). Though the heating rate at the lower region of the left wall is much higher than at the top, the pressure profiles at the three locations are insensitive to the variation. The effect of spatially nonuniform gradual heating

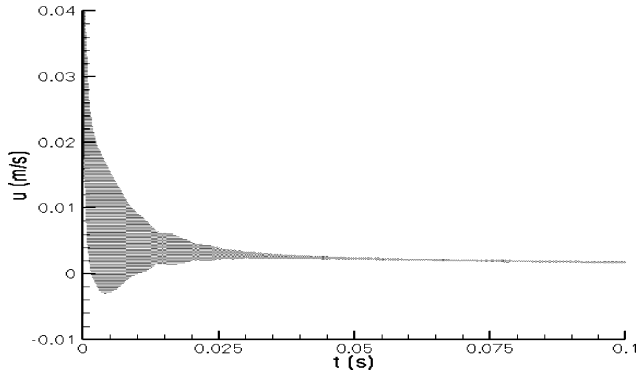

Fig. 8 Variation of x component of velocity with time at midpoint of enclosure, under spatially uniform gradual heating, $\tau_h = 5\tau_c$, zero gravity.

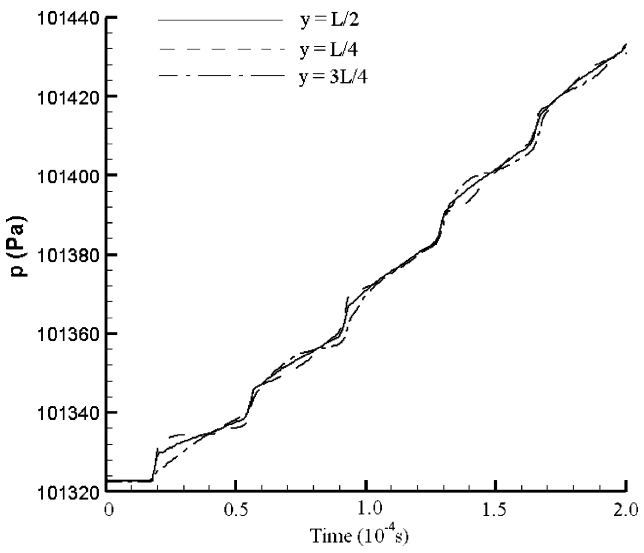

Fig. 9 Variation of pressure with time for three points at midline of enclosure, under spatially nonuniform gradual heating $\tau_h = 5\tau_c$, zero gravity.

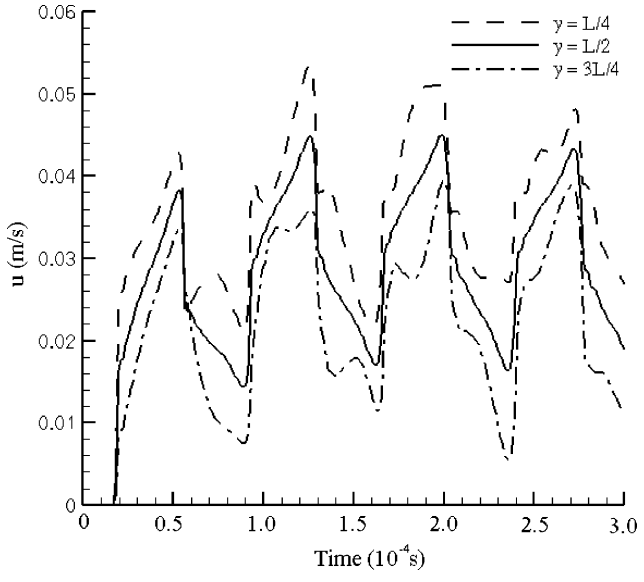

Fig. 10 Variation of x component of velocity with time for three points at midline of enclosure, under spatially nonuniform gradual heating $\tau_h = 5\tau_c$, zero gravity.

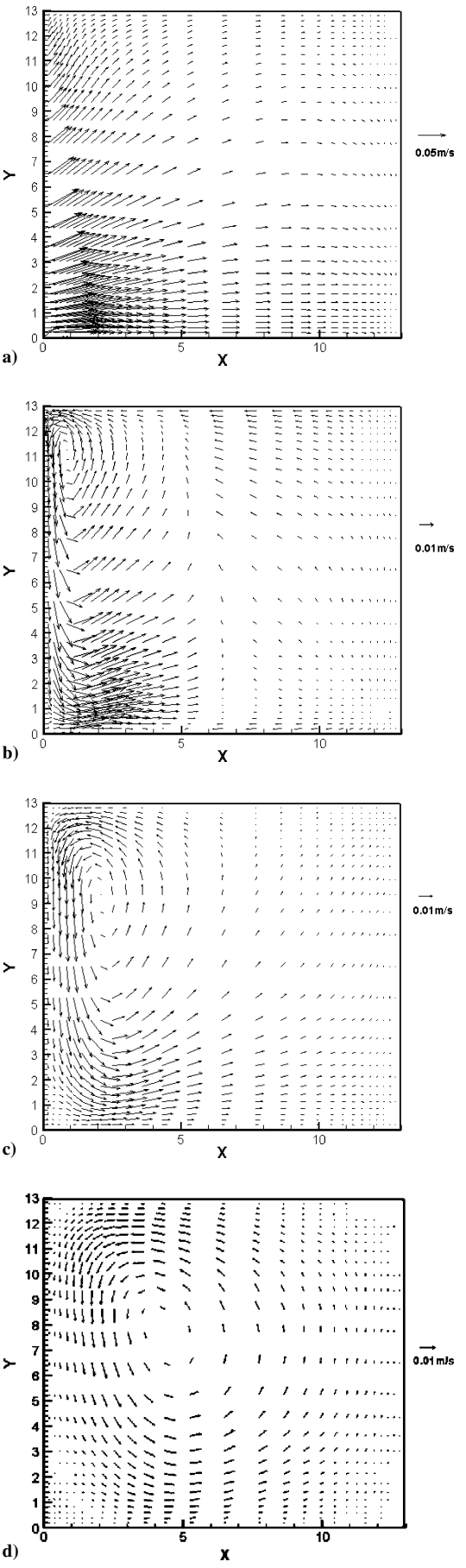

Fig. 11 Velocity vectors under spatially nonuniform gradual heating $\tau_h = 5\tau_c$, zero gravity: a) 0.074 ms, b) 7.37 ms, c) 25.78 ms, and d) 100 ms.

on the x component of the velocity, as shown in Fig. 10, is quite different. The x component of velocity values fluctuates with time, however, does not reverse sign (as was shown in Fig. 3). Hence, the damping rate is slower in this case (gradual heating) than the impulsive heating cases. The x component of velocity is highest at $y = L/4$ because the heating rate is higher at the lower region of the left wall.

Figures 11a–11d show the development of velocity vectors from 0.074 to 100 ms. At 0.074 ms, (Fig. 11a) all fluid flows in the direction nearly normal to the vertical wall because the pressure disturbance is generated in the horizontal direction. Figure 11a also shows that the horizontal velocity in the lower region of the enclosure (with higher wall temperature) is higher than that in the upper region, which demonstrates that the thermoacoustic wave-induced flow strength is proportional to the temperature increase on the wall. At a later time, 7.37 ms, there is a recirculating flow pattern at the left top corner, as shown in Fig. 11b. With increasing time, this vortical flowfield grows and covers the entire enclosure. Even at 100 ms, the flowfield is quite strong. We saw earlier that spatially uniform gradual heating can generate a longer lasting flowfield than impulsive heating with the same overheat ratio. Here we see that the strength of this flowfield can be further be enhanced with spatially nonuniform heating.

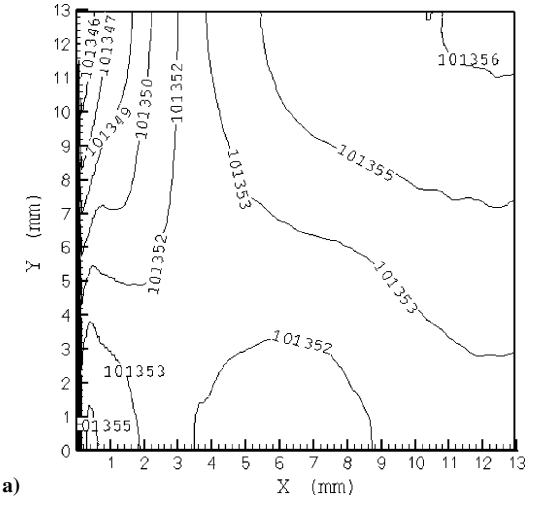

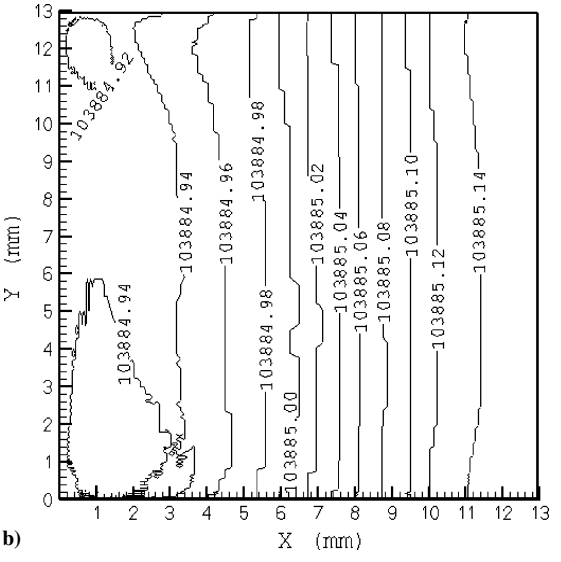

Fig. 12 Pressure contours under spatially nonuniform gradual heating $\tau_h = 5\tau_c$, zero gravity: a) $P_{\min} = 101345.44$ Pa, $P_{\max} = 101362.58$ Pa, and $\pm = 0.074$ ms and b) $P_{\min} = 103884.92$ Pa, $P_{\max} = 103885.14$ Pa, and $\pm = 25$ ms.

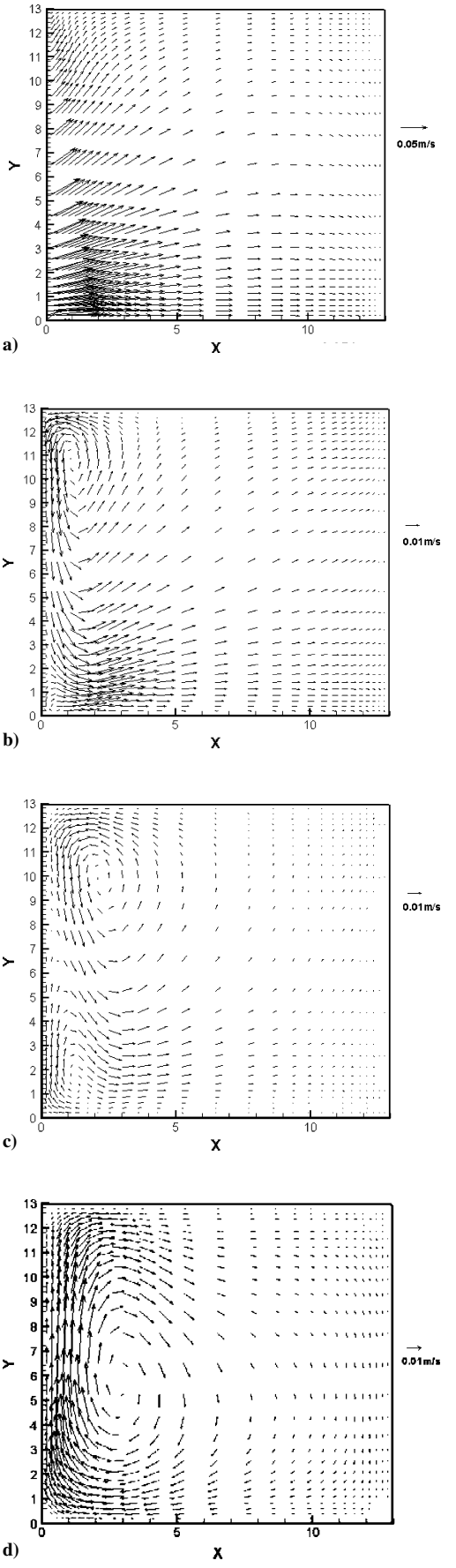

Fig. 13 Velocity vectors under spatially nonuniform gradual heating $\tau_h = 5\tau_c$, normal gravity: a) 0.074 ms, b) 7.37 ms, c) 25.78 ms, and d) 100 ms.

Table 1 Summary of main observations

Case	Description	Short-term observations	Long-term observations
A	Uniform impulsive heating, 0 *g*	1) Strong thermoacoustic waves 2) Horizontal velocity component reverses sign after reflection from a sidewall	1) Essentially one-dimensional flowfield 2) The damping rate for the flowfield is high
B	Uniform gradual heating, 0 *g*	1) Weak pressure (thermoacoustic) waves 2) Horizontal velocity component fluctuates in value after reflection from a sidewall but does not reverse sign	1) Two-dimensional flowfield is developed, near the corners of the heated wall 2) Damping rate for the flowfield is slow
C	Nonuniform gradual heating, 0 *g*	1) Thermoacoustic wave speed insensitive to the variation of the heating rate along the vertical direction 2) Horizontal velocity component values are higher at the lower region of the enclosure (higher heating rate)	1) Two-dimensional counter-clockwise vortical flowfield is established 2) Damping rate for the flowfield is low
D	Nonuniform gradual heating, 1 *g*	1) No gravity effects 2) Thermoacoustic wave aped is insensitive to the variation of the heating rate along the vertical direction 3) Horizontal velocity component values are higher at the lower region of the enclosure (higher heating rate)	1) Effect of gravity (buoyancy) becomes evident 2) The counter-clockwise flowfield created by thermoacoustic waves replaced by a strong clockwise vortical flow. 3) Overall strength of the flowfield at 100 ms similar to that observed in case C.

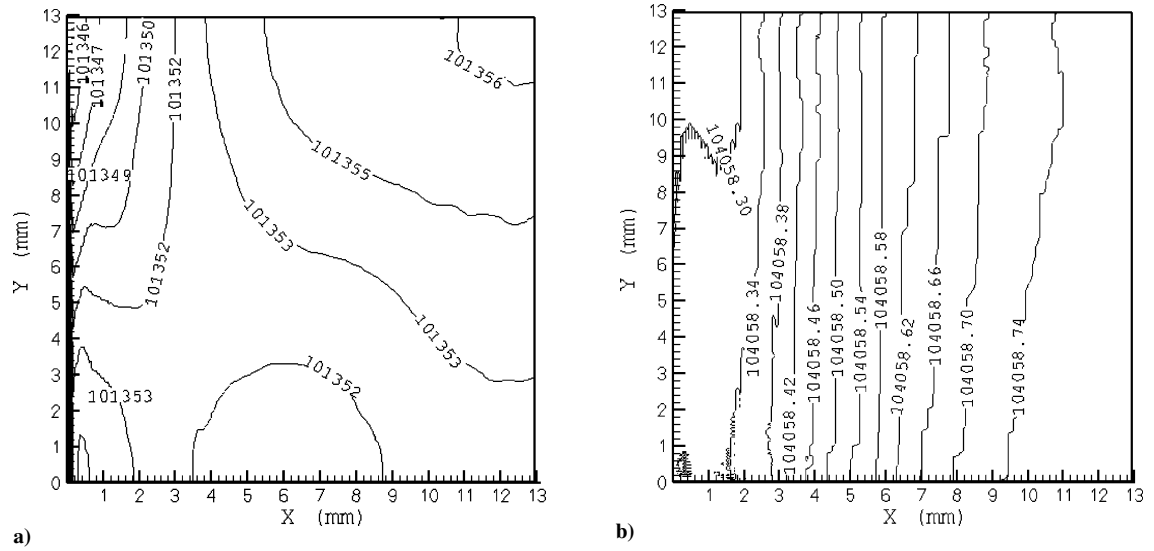

Fig. 14 Pressure contours under spatially nonuniform gradual heating $\tau_h = 5\tau_c$, normal gravity: a) $P_{min} = 101345.44$ Pa, $P_{max} = 101362.58$ Pa, and $t = 0.074$ ms and b) $P_{min} = 104058.30$ Pa, $P_{max} = 104058.74$ Pa, and $\pm = 25$ ms.

Pressure contours at two different times are shown in Fig. 12. At the early time ($t = 0.074$ ms), a strong pressure difference, 17.14 Pa, was found in the whole flowfield due to the generation of thermoacoustic wave that is nonuniform in the vertical direction. At $t = 25$ ms, however, the pressure difference decreases to 0.22 Pa, and the pressure difference in the vertical direction also disappears except in the region near the left wall, where an eddy is developed.

D. Spatially Nonuniform Gradual Heating Under Normal Gravity

Now we consider the effect of gravity on the flows induced by thermoacoustic waves. The conditions considered here identical to those considered in Sec. III. C, albeit at normal-gravity conditions. Figures 13a–13d show the development of velocity vectors in the enclosure from 0.074 to 100 ms. At $t = 0.074$ ms (Fig. 13a) and $t = 7.37$ ms (Fig. 13b), the predicted flowfields are similar to the results shown in Figs. 11a and 11b under zero-gravity conditions. The buoyancy-induced flow takes a comparatively larger time to develop than the thermoacoustic wave-induced flows. The flowfield shown in Fig. 13c at $t = 25.78$ ms shows the signs of a developing buoyancy-induced flow along the left lower corner of the enclosure. With increasing time, $t = 100$ ms, (Fig. 13d), this vortical flowfield grows and finally covers the entire enclosure. The overall strength of the flowfield in the enclosure at $t = 100$ ms under zero- (Fig. 11d) and normal-gravity (Fig. 13d) conditions is quite similar. The direction of the vertical flow, however, is in opposite directions. With increasing time, the flowfield under normal-gravity conditions will represent a purely buoyancy-induced flowfield, and the flowfield under zero gravity conditions will damp out.

Pressure contours at two different times, under normal-gravity, nonuniform heating conditions are shown in Fig. 14. The pressure contours at early time, $t = 0.074$ ms (Fig. 14a), is identical to that for the zero-gravity case (Fig. 12a). A large pressure difference, 17.14 Pa, was found in the flowfield, due to the generation of the thermoacoustic waves. At $t = 25$ ms (Fig. 14b), however, the overall pressure difference decreases to about 0.22 Pa. When compared with the zero gravity case (Fig. 12b), the pressure near the left wall is low along the vertical direction because of the development of the buoyancy-induced flow.

Observations of the short-term and long-term responses of the enclosure fluid due to the four types of heating conditions considered are listed in Table 1.

IV. Summary

Thermoacoustic wave-induced flowfields in an enclosure were studied by solving the unsteady compressible Navier–Stokes equations. The effects of the pressure (thermoacoustic) waves on flow

development were determined by using a highly accurate FCT algorithm. Thermoacoustic waves were generated by increasing the left-wall temperature of the enclosure impulsively (suddenly) or gradually. The rapidity of the wall heating process was found to be the main parameter determining the strength of the thermoacoustic waves. The effects of spatially nonuniform heating of the wall on the developed flowfield were also studied.

Table 1 summarizes the results for the cases studied. Impulsive heating generates strong thermoacoustic waves; however, the damping rate for the resulting velocity field is high. Gradual heating produced weaker thermoacoustic waves, but they tend to produce flowfields that can remain for longer periods. Spatially nonuniform heating produced faster flows in the region with higher heating and eventually resulted in recirculating flowfields in the enclosure. For the conditions studied, the effect of gravity on the flowfields is only evident after about 25 ms from the start of the heating process. The strength of buoyancy-induced flowfield at 100 ms was similar to that obtained by thermoacoustic wave-induced flow at zero gravity.

Acknowledgment

The authors gratefully acknowledge support from NASA Grants NNC04AA22A and NNC04IA09I.

References

[1]Churchill, S. W., and Brown, M. A., "Thermoacoustic Convection and the Hyperbolic Equation of Conduction," *International Communications in Heat and Mass Transfer*, Vol. 14, No. 6, 1987, pp. 647–655.

[2]Farouk, B., Oran, E. S., and Fusegi, T., "Numerical Study of Thermoacoustic Waves in an Enclosure," *Physics of Fluids*, Vol. 12, No. 5, 2000, pp. 1052–1061.

[3]Huang, Y., and Bau, H. H., "Thermoacoustic Waves in a Semi-Infinite Medium," *International Journal of Heat and Mass Transfer*, Vol. 38, No. 8, 1995, pp. 1329–1345.

[4]Huang, Y., and Bau, H. H., "Thermoacoustic Waves in a Confined Medium," *International Journal of Heat and Mass Transfer*, Vol. 40, No. 2, 1997, pp. 407–419.

[5]Parang, M., "An Experimental and Analytical Investigation of Thermoacoustic Convection Heat Transfer in Gravity and Zero-Gravity Environments," NASA Final Rept., Grant NAG3-239, July 1986.

[6]Parang, M., and Salah-Eddine, A., "Experiments on Thermoacoustic Convection Heat Transfer in Gravity and Low Gravity Environments," AIAA Paper 87-1651, Jan. 1987.

[7]Parang, M., and Salah-Eddine, A., "Thermoacoustic Convection Heat-Transfer Phenomenon," *AIAA Journal*, Vol. 22, No. 7, 1984, pp. 1020–1022.

[8]Brown, M. A., and Churchill, S. W., "Experimental Measurements of Pressure Waves Generated by Impulsive Heating of a Surface," *AIChE Journal*, Vol. 41, No. 2, 1995, pp. 205–213.

[9]Brown, M. A., and Churchill, S. W., "Finite-Difference Computation of the Wave Motion Generated in a Gas by a Rapid Increase in the Bounding Temperature," *Computers and Chemical Engineering*, Vol. 23, Sept. 1999, pp. 357–376.

[10]Trilling, L., "On Thermally Induced Sound Fields," *Journal of the Acoustical Society of America*, Vol. 27, No. 3, 1955, pp. 425–431.

[11]Ozoe, H., Sato, N., and Churchill, S. W., "The Effect of Various Parameters on Thermoacoustic Convection," *Chemical Engineering Communications*, Vol. 5, Aug. 1980, pp. 203–221.

[12]Ozoe, H., Sato, N., and Churchill, S. W., "Numerical Analyses of Two and Three Dimensional Thermoacoustic Convection Generated by a Transient Step in the Temperature of One Wall," *Numerical Heat Transfer*, Pt. A, Vol. 18, March 1990, pp. 1–15.

[13]Aktas, M. K., and Farouk, B., "Numerical Simulation of Developing Natural Convection in an Enclosure due to Rapid Heating," *International Journal of Heat and Mass Transfer*, Vol. 46, No. 7, 2003, pp. 2253–2261.

[14]Zappoli, B., Amiroudine, S., Carles, P., and Ouazzani, J., "Thermoacoustic and Buoyancy-Driven Transport in a Square Side-Heated Cavity Filled with a Near-Critical Fluid," *Journal of Fluid Mechanics*, Vol. 316, 1996, pp. 53–72.

[15]Kays, W. M., and Crawford, M. E., *Convective Heat and Mass Transfer*, 1993, McGraw–Hill, New York, Appendix A.

[16]Boris, J. P., Landsberg, A. M., Oran, E. S., and Gardner, J. H., "LCPFCT—A Flux-Corrected Transport Algorithm for Solving Generalized Continuity Equations," Naval Research Lab., Rept. NRL/MR/6410-93-7192, Washington, DC, Dec. 1993.

[17]Poinsot, T. J., and Lele, S. K., "Boundary Conditions for Direct Simulations of Compressible Viscous Flows," *Journal of Computational Physics*, Vol. 101, 1992, pp. 104–129.